Electro-optical Kerr effect in HFE-7100

Michelle Nassar, Michel Daaboul, Anny Michel, Christophe Louste

▶ **To cite this version:**

Michelle Nassar, Michel Daaboul, Anny Michel, Christophe Louste. Electro-optical Kerr effect in HFE-7100. 2023 IEEE 22nd International Conference on Dielectric Liquids (ICDL), Jun 2023, Worcester, United States. pp.1-4, 10.1109/ICDL59152.2023.10209331 . hal-04428695

HAL Id: hal-04428695

https://univ-poitiers.hal.science/hal-04428695v1

Submitted on 31 Jan 2024

HAL is a multi-disciplinary open access archive for the deposit and dissemination of scientific research documents, whether they are published or not. The documents may come from teaching and research institutions in France or abroad, or from public or private research centers.

L'archive ouverte pluridisciplinaire **HAL**, est destinée au dépôt et à la diffusion de documents scientifiques de niveau recherche, publiés ou non, émanant des établissements d'enseignement et de recherche français ou étrangers, des laboratoires publics ou privés.

Electro-optical Kerr effect in HFE-7100

Michelle Nassar
Energy Management Business
Schneider Electric
Grenoble, France
michelle.nassar@se.com

Michel Daaboul
Dept. of Mechanical Engineering
University of Balamand
Al Kurah, Lebanon
michel.daaboul@balamand.edu.lb

Anny Michel
Dept. Physqiue et Mécanique des Matériaux
Pprime Institute
Poitiers, France
anny.s.michel@univ-poitiers.fr

Christophe Louste
Dept. Fluide, Thermique et Combustion
Pprime Institute
Poitiers, France
christophe.louste@univ-poitiers.fr

***Abstract*—This work is an experimental study on electro-optical Kerr effect in hydrofluoroether HFE-7100. It is part of a scientific project aiming to better understand electrohydrodynamic (EHD) behavior and hence optimize EHD systems. The electro-optical Kerr effect is a nonintrusive method that allows to study the development of charged layers at the electrode/liquid interface. In this paper, the authors examine the applicability of the Kerr effect method on HFE-7100, a dielectric liquid that has proven to be very efficient in EHD applications. The system consists of a monochromatic green laser source and a rectilinear polariscope. The Kerr cell has two planar electrodes on which a high sinusoidal voltage is applied. The light intensity of the obtained images is then analyzed. The Kerr coefficient value B of the HFE-7100 is deduced to be $B = 2.7\times10^{-14}$V/m², a value that is comparable to that of purified water. Kerr images are presented, and their qualitative analysis demonstrates the presence of space charge. This work proves that HFE has a good sensitivity to the Kerr effect.**

Keywords— Dielectric liquid, electric charges, electric field distribution, electrohydrodynamics, electro-optical Kerr effect, hydrofluoroether, Kerr coefficient, Kerr image, polariscope.

I. Introduction

Electrohydrodynamic (EHD) systems are based on the principle of setting a dielectric liquid in motion by the simple application of an electric field. The forces used in EHD depend on the nature of the charged layers formed at the liquid/electrode interfaces, as well as on the charge density produced. A better understanding of the physical phenomena of charge development will contribute to the design of more accurate numerical models and thus to the optimization of EHD systems.

The aim of this work is to study the development of charged layers by a non-intrusive method called the electro-optical Kerr effect. This method is based on the principle of making a dielectric liquid birefringent under the effect of an applied electric field. It consists in illuminating the test cell and then recording the light intensity of the images produced. The gray levels in the images obtained provide information on the spatial distribution of the electric field and hence can be used to calculate the charge density.

Several authors, such as Denat [1] and Tobazéon [2] have contributed to the development of this technique. Zahn and his team at MIT used Kerr effect to analyze space charges under the application of high voltages through their numerous studies initially conducted on nitrobenzene [3], [4] (of Kerr coefficient $B_{nitrobenzene}\approx3.5\times10^{-12}$m/V²).

Although it is particularly sensitive to the Kerr effect with a very high Kerr coefficient, nitrobenzene is not the only liquid to have been studied, especially in view of its toxicity. In particular, Zahn used the Kerr effect to study the distribution of electric field and that of space charges in the vicinity of electrodes immersed in ultra-purified water [5]–[8] ($B_{water}\approx3.4\times10^{-14}$m/V²). Some studies on transformer oils can also be found [9]–[12] ($B_{oil}\approx1.8\times10^{-15}$m/V²).

There are no examples in the literature of the application of the electro-optical Kerr effect on Hydrofluoroethers (HFE), which are dielectric liquids that have proven to be very efficient in EHD applications [13], [14]. Therefore, this study mainly seeks to test the applicability of this method on HFE-7100.

II. Experimental Setup

There are several types of polariscopes which differ in their configurations. A rectilinear polariscope with crossed polarizers is used in this study. The Kerr cell was designed in the Pprime laboratory. A schematic representation of this cell is given in Fig. 1. It is composed of a cylindrical glass enclosure and two flat electrodes immersed in HFE-7100. The electrodes are stainless steel parallel plates, with a length L=15cm. The inter-electrode distance d is fixed at 5mm. The cell is designed to be sealed and thus it can limit the loss of the liquid by evaporation, knowing that HFEs are highly volatile. The left electrode is connected to a high voltage source, while the right electrode is connected to ground.

The instruments of the high voltage generation and measurement system include the GBF function generator, the TREK voltage amplifier, and an oscilloscope. The latter is a Teledyne LeCroy WaveSurfer 3024 series four-channel digital oscilloscope with a bandwidth of 200MHz and a sampling rate of 4G samples/s.

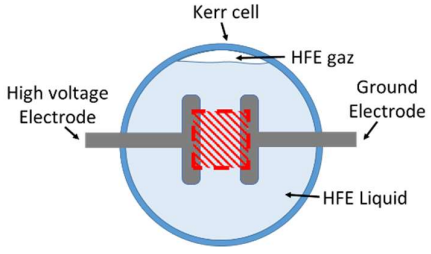

Fig. 1. Schematic representation of the Kerr cell

XXX-X-XXXX-XXXX-X/XX/$XX.00 ©20XX IEEE

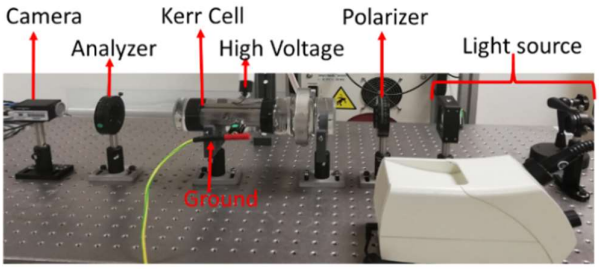

Fig. 2. Photo of the rectilinear polariscope used for the experimental setup

The optical system consists of a green laser with wavelength λ=532nm. The parallel illumination of the laser is provided by a beam expander, which can expand up to 20 times, allowing hence the coverage of the whole electrode gap. The rectilinear polariscope shown in Fig. 2 consists of two polarizers and a camera. The camera is limited to 80fps and has a maximum resolution of 2048×2048 pixels. The red hatched rectangle on Fig. 1 symbolizes the position of the image taken by the camera.

III. Experimental Protocol

Kerr measurements were performed in a clean room environment to limit dust deposition on the optical elements. The cell was cleaned as much as possible and was rinsed with HFE-7100 to remove impurities and particles that can cause premature breakdown and reduce the accuracy of optical detection. Then, the cell was filled completely with liquid to avoid bubble formation and undesirable optical effects on the liquid surface.

Before each measurement, a Malus law was performed by fixing the angle of the polarizer and varying the angle of the analyzer with steps of 5°. This law states that the measured light intensity I describes a curve of type cos² as described in (1), with θ being the angle between the polarizer and the analyzer, and I_1 being the light intensity at the output of the polarizer.

$$I(\theta)=I_1(\cos\theta)^2 \tag{1}$$

According to (1), I is maximal when θ=0° (aligned polarizers) and null when θ=90° (crossed polarizers). In this way, Malus' law could be used to measure the light intensity I_0 in the absence of field. This procedure served as a calibration for Kerr measurements.

After performing Malus' law, the analyzer and polarizer of the rectilinear polariscope were fixed to be crossed. To obtain maximum intensity with a rectilinear polariscope, the angle α of the polarizer was set to $\pi/4$ and the angle β of the analyzer to $3\pi/4$. The equation that corresponds to this configuration of polariscope is:

$$I/I_0=\sin^2(\pi BLE^2) \tag{2}$$

Where B is the liquid's Kerr coefficient, and E is the electric field applied.

Measurements were then made by applying a high sinusoidal voltage, and the images were captured by the camera. Once the measurements were completed, a Malus law was performed again to ensure that the light intensity level has not changed.

It must be noted that all tests were performed at room temperature of 22°C.

IV. Experimental Results

A. Malus' law and calibration

An example of a Malus' law performed as described in the previous section is given in Fig. 3. The experimental measurement points were obtained by averaging the light intensity of the central area of the obtained image. Several area sizes were tested ranging from 10×10 to 550×550 pixels, but only four cases (50×50, 100×100, 150×150 and 200×200 pixels) are represented here.

The points corresponding to the measurements are represented with symbols while the theoretical curve obtained according to (1) is represented with a black solid line. The similarity of the experimental curves found by averaging different area sizes shows that this averaging method is quite satisfactory. Fig. 3 shows the good consistency between the theoretical model of Malus' law and the experimentally performed measurements. The graphs in Fig. 3 also show that the minimum value of measured light intensity is I_{min}=38 gray levels. That means that the camera detects some light even at θ=90°, where should have been total extinction. In addition to that, it can be seen on the graphs that when the two polarizers are aligned (at θ=0°), the maximum value of measured light intensity is I_{max}=160 gray levels. Equation (2) is therefore corrected accordingly:

$$I/I_0=\sin^2(\pi BLE^2)+A \tag{3}$$

Where A is a constant.

If $\sin^2(\pi BLE^2)=1$ then $I=I_{max}$, and thus:

$$I_{max}=(1+A)I_0 \tag{4}$$

If $\sin^2(\pi BLE^2)=0$ then $I=I_{min}$, and thus:

$$I_{min}=AI_0 \tag{5}$$

From (4) and (5), it can be deduced that: $I_0=I_{max}-I_{min}$ and $A=I_{min}/I_0$. Substituting these values into (3), the following equation is obtained:

$$\frac{I}{I_{max}-I_{min}}=\sin^2(\pi BLE^2)+\frac{I_{min}}{I_{max}-I_{min}} \tag{6}$$

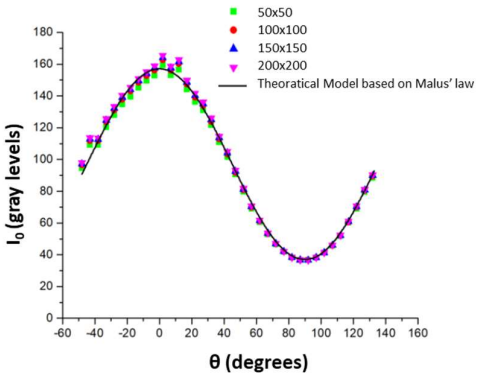

Fig. 3. Superposition of the experimental data and the theoratical model of the measured light intensity in the absence of electric field in function of θ

And hence the equation becomes:

$$\frac{I-I_{min}}{I_{max}-I_{min}} = \sin^2(\pi BLE^2) \quad (7)$$

B. Calculation of the Kerr coefficient of HFE-7100

The measurements presented here correspond to an application of a sinusoidal voltage of maximum value V_{max}=30kV and a frequency f of 2Hz to electrodes spaced of d=5 mm. The tests were performed at low frequencies to avoid heating of the liquid.

In her work, Nassar showed that, for HFE-7100, the charged layers start developing around a frequency of 0.1Hz under a constant field of about 570V/m [15]. Thus, for the voltage case applied here, the charged layers should have sufficient time to develop.

Equation (2) can be used to find the value of B. With the sinusoidal signal applied, the applied electric field is written:

$$E=\frac{V_{max}}{d}\sin(2\pi ft+\phi_0) \quad (8)$$

Where t is the time, and ϕ_0 is an angle to compensate for the frequency of the applied signal.

Equation (2) becomes:

$$\frac{I}{I_0} = \sin^2(\pi BL\left(\frac{V_{max}}{d}\right)^2 \sin^2(2\pi ft+\phi_0)) \quad (9)$$

The method of averaging the light intensity I from a central area in the middle of the electrodes was chosen since the central area in the middle of the electrodes is the area least affected by the field variation due to charging phenomena. The area size chosen here for the calculation of the Kerr coefficient is 150×150 pixels.

A phase analysis is performed on the experimental data. The value of B can be determined using (9) in such a way to have the best fit of the theoretical curve to the experimental data. The calculation results in a value of $B = 2.7\times10^{-14}$m/V^2.

In Fig. 4 are represented in black symbols the experimental data and in red solid line the theoretical model obtained with B=2.7×10^{-14}m/V^2.

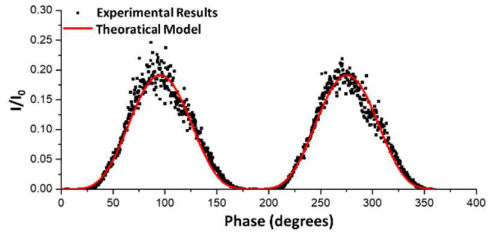

Fig. 4. Superposition of the experimental data with the theoretical model calculated with B=2.7×10^{-14}m/V^2. The phase given on the x-axis corresponds to ($2\pi ft+\phi_0$) in equation (9)

As can be seen in Fig. 4, the experimental data show a variation in the form of a sin^2 curve, a sign of the presence of the Kerr effect. I/I_0 reaches a maximum value of about 0.22 in this setup. We can see that the agreement with the theoretical model is not perfect; it is very slightly shifted with respect to the experimental data. This may be due to the presence of the charged layers which can affect the measurement by locally changing the value of the electric field. However, the model remains a good approximation of the experimental data.

C. Electro-optical Kerr images in HFE-7100

The measurements shown here correspond to the same sinusoidal voltage with V_{max}=30kV and f=2Hz.

Before analyzing the images, a recall of the link between Kerr images and electric field distribution is given:

According to Thomson's model, the presence of space charges, and depending on their type, locally varies the electric field between the electrodes [16]. In case of the absence of charged layers (when the voltage is sufficiently low), the electric field is constant between the two parallel electrodes. On a Kerr image, this means that the light intensity will be homogeneous between the electrodes. On the other hand, if the light intensity is not homogeneous, this indicates a variation in electric field and therefore the presence of space charges. A more intense area of light corresponds to a locally higher electric field, and vice versa.

Fig. 5 and Fig. 6 represent two Kerr images obtained at t=0.24T and t=0.69T, respectively, with T being the period of the signal applied. In the pictures, the electrodes appear as black areas on the left and right. They are delimited by red lines The area in the center contains the liquid. The sign of each electrode is noted in red at the top of the images.

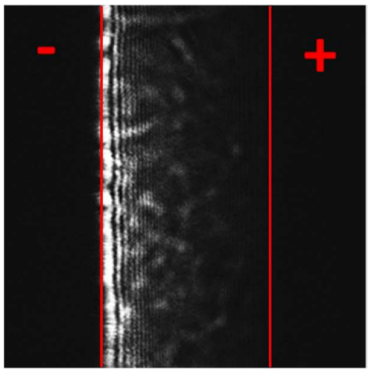

Fig. 5. Kerr image obtained under a sinusoidal voltage of V_{max}=30kV and f=2Hz in a crossed rectilinear polarsicope steup at t=0.24T

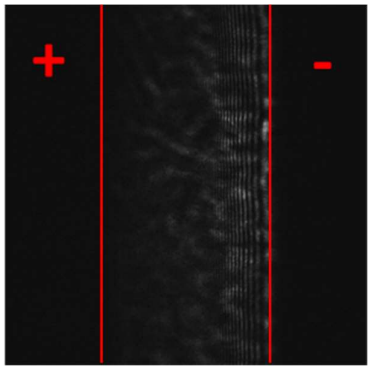

Fig. 6. Kerr image obtained under a sinusoidal voltage of V_{max}=30kV and f=2Hz in a crossed rectilinear polarsicope steup at t=0.69T

Both images show the emergence of fringes and an inhomogeneous spatial distribution of light. It can be observed that the light intensity of the fringes is the highest near the negative electrode/liquid interface, and then it decreases

gradually until total extinction near the positive electrode/liquid interface. Moreover, the light in Fig. 5 has a stronger light intensity than the one in Fig. 6. This is because Fig. 6 represents a time t on the applied sinusoidal signal where the voltage (and thus the electric field) is smaller. In fact, Fig. 5 corresponds to V=29.9kV whereas Fig. 6 corresponds to V=27.9kV.

As per the above-mentioned analysis, these observations demonstrate an inhomogeneous spatial distribution of the electric field between the two parallel electrodes, and hence the presence of space charges in the liquid.

The central zone in the middle of the electrodes remains the darkest and with the most homogeneous light intensity. Indeed, this zone is the least affected by the variations of the field induced by the presence of space charges.

The analysis presented here is only a qualitative description of the images. A quantitative analysis will be done in a future work to affirm these results.

V. Conclusion

The electro-optical Kerr effect is based on the principle of making a liquid birefringent under the effect of an applied electric field. Thus, a light passing through the medium will change its polarization state at the exit of the Kerr cell. The analysis of the light intensity in the obtained images gives information about the spatial distribution of the electric field. In this way, the Kerr effect allows to study the development of charged layers at the electrode/liquid interfaces.

This method has been successfully used by several researchers for the measurement of space charges in nitrobenzene, ultra-purified water and even in transformer oil. Knowing that the measurement of charged layers is extremely important for the optimization of EHD systems, this study focuses on examining the applicability of the Kerr effect method on HFE-7100.

In this work, the device is a rectilinear polariscope consisting of a Kerr cell with planar electrodes of length 15cm and a gap of 5mm. The light source used is a monochromatic green laser. Before each measurement, a calibration by Malus law is performed by varying the angle θ between the polarizer and the analyzer. This method allows to measure the value of the maximum intensity I_0 in the absence of electric field. After that, a configuration of the polariscope with crossed polarizers is set. A high sinusoidal voltage is applied, and the images are recorded by the camera.

The Kerr coefficient value of the HFE-7100 is deduced using a 150×150 pixel area in the middle of the image. In this central area, the light intensity remains homogeneous, and the electric field is least affected by the development of charged layers. The calculation results in B=2.7×10^{-14}m/V^2. Compared to other liquids in the literature, HFE-7100 is found to have a Kerr coefficient of the same order of magnitude as purified water (B_{water}≈3.4×10^{-14}m/V^2). Thus, the HFE is proven to have good sensitivity to the Kerr effect.

Finally, two Kerr images are presented. A qualitative analysis of the images shows the presence of charges in the liquid. Calculating the spatial distribution of the field from the results is not immediate but will be done in a future work. The study has demonstrated the feasibility of the Kerr effect space charge measurement method in HFE-7100. This technique should work with other HFEs, and the studies could be extended.

Acknowledgment

This work was funded in the framework of the French government program «Investissements d'Avenir», (LABEX INTERACTIFS reference ANR-11-LABX-0017-01).

References

[1] A. Denat, "Etude de la conduction électrique dans les solvants non polaires," Université Joseph-Fourier, Grenoble, 1982.

[2] R. Tobazéon, "Etude du transfert convectif de charges électriques par un jet de liquide isolant et application à la génération de tensions élevées," Université Joseph-Fourier, Grenoble, 1973.

[3] M. Zahn, "Electro-optic field and space-charge mapping measurements in high-voltage stressed dielectrics," *Physics in Technology*, vol. 16, no. 6, p. 288, Nov. 1985, doi: 10.1088/0305-4624/16/6/I03.

[4] M. Zahn, "Space Charge Effects in Dielectric Liquids," in *The Liquid State and Its Electrical Properties*, E. E. Kunhardt, L. G. Christophorou, and L. H. Luessen, Eds. Boston, MA: Springer US, 1988, pp. 367–430. doi: 10.1007/978-1-4684-8023-8_16.

[5] M. Zahn, "Optical, electrical, and electro-mechanical measurement methodologies of electric field, charge, and polarization in dielectrics," in *1998 Annual Report Conference on Electrical Insulation and Dielectric Phenomena (Cat. No.98CH36257)*, 1998, vol. 1, pp. 1–14 vol. 1. doi: 10.1109/CEIDP.1998.733834.

[6] M. Zahn, Y. Ohki, K. Rhoads, M. LaGasse, and H. Matsuzawa, "Electro-Optic Charge Injection and Tramsport Measurements in Highly Purified Water and Water/Ethylene Glycol Mixtures," *IEEE Transactions on Electrical Insulation*, vol. EI-20, no. 2, pp. 199–211, 1985, doi: 10.1109/TEI.1985.348821.

[7] M. Zahn, T. Takada, and S. Voldman, "Kerr electro-optic field mapping measurements in water using parallel cylindrical electrodes," *Journal of Applied Physics*, vol. 54, no. 9, pp. 4749–4761, 1983, doi: 10.1063/1.332809.

[8] M. Zahn and T. Takada, "High voltage electric field and space-charge distributions in highly purified water," *Journal of Applied Physics*, vol. 54, no. 9, pp. 4762–4775, 1983, doi: 10.1063/1.332810.

[9] N. Inoue, M. Wakamatsu, K. Kato, H. Koide, and H. Okubo, "Charge accumulation mechanism in oil/pressboard composite insulation system based on optical measurement of electric field," *IEEE Transactions on Dielectrics and Electrical Insulation*, vol. 10, no. 3, pp. 491–497, 2003, doi: 10.1109/TDEI.2003.1207477.

[10] K. Nakamura, K. Kato, H. Koide, Y. Hatta, and H. Okubo, "Fundamental property of electric field in rapeseed ester oil based on Kerr electro-optic measurement," *IEEE Transactions on Dielectrics and Electrical Insulation*, vol. 13, no. 3, pp. 601–607, 2006, doi: 10.1109/TDEI.2006.1657974.

[11] S. Yamamoto, K. Kato, F. Endo, Y. Hatta, H. Koide, and H. Okubo, "Kerr electro-optic field measurement in palm oil fatty acid ester transformer insulation system," in *2007 Annual Report - Conference on Electrical Insulation and Dielectric Phenomena*, 2007, pp. 784–787. doi: 10.1109/CEIDP.2007.4451461.

[12] F. O'Sullivan *et al.*, "Modeling the Effect of Ionic Dissociation on Charge Transport in Transformer Oil," in *2006 IEEE Conference on Electrical Insulation and Dielectric Phenomena*, 2006, pp. 756–759. doi: 10.1109/CEIDP.2006.312042.

[13] M. Talmor, C. Louste, and J. Seyed-Yagoobi, "PIV flow field measurements of electrohydrodynamic conduction pumping," in *Proc. of the 2018 Electrostatics Joint Conference Conf*, 2018, pp. 1–15.

[14] M. Daaboul, P. Traoré, P. Vázquez, and C. Louste, "Study of the transition from conduction to injection in an electrohydrodynamic flow in blade-plane geometry," *Journal of Electrostatics*, vol. 88, pp. 71–75, 2017, doi: https://doi.org/10.1016/j.elstat.2017.01.014.

[15] M. Nassar, "Caractérisation des propriétés électriques et des coefficients Kerr de deux hydrofluoroethers utilisés en électrofluidodynamique," PhD Thesis, 2021. [Online]. Available: http://www.theses.fr/2021POIT2304/document

[16] *Conduction of electricity through gases*, 3rd ed., vol. II. Cambridge: Cambridge University Press, 1933.